Innovative additive manufacturing solutions for fabrication of aerodynamic test models

Szymon Żydowski [1], Maciej Pilch [1], Joanna Ortyl [2], Andrzej Flaga[1]

[1] *Cracow University of Technology, Faculty of Civil Engineering, Wind Engineering Laboratory, Warszawska 24, 31-155 Kraków, Poland, sz.zydowski@gmail.com*

[2] *Cracow University of Technology, Faculty of Chemical Engineering and Technology, Warszawska 24, 31-155 Kraków, Poland joanna.ortyl@pk.edu.pl*

SUMMARY

Accurate surface pressure measurement in boundary-layer wind tunnel (BLWT) experiments is fundamental to the assessment of wind-induced loads on civil structures including buildings, bridges, and industrial facilities and to the validation of numerical models used in structural wind engineering design. The reliability of such measurements depends critically on the aerodynamic fidelity and pressure-tap integration of the physical test models deployed in the wind tunnel. This paper presents an innovative fabrication methodology for fully instrumented aerodynamic models using Digital Light Processing (DLP) additive manufacturing, in which complete pressure channel networks are embedded directly within the model body as monolithic structures during a single fabrication cycle, eliminating the geometric and structural constraints imposed by conventional post-fabrication drilling A dedicated photopolymer resin was developed to address DLP printing failures in enclosed channels, featuring a high density-to-viscosity ratio currently under patent preparation.

Keywords: wind tunnel testing, aerodynamic pressure measurement, additive manufacturing, DLP, photopolymer, boundary-layer wind tunnel

1. INTRODUCTION

The determination of wind-induced pressure distributions on civil structures constitutes one of the central objectives of experimental wind engineering. Building codes and standards — including EN 1991-1-4 and its national annexes — provide codified pressure coefficient data for canonical structural forms, but the aerodynamic behavior of geometrically complex or site-sensitive structures frequently lies outside the scope of codified guidance, necessitating direct experimental determination through wind tunnel testing. Boundary-layer wind tunnel (BLWT) experiments, in which scale models of the target structure are exposed to a simulated atmospheric boundary layer flow, remain the accepted method for obtaining the surface pressure data required for cladding design, structural load assessment, and pedestrian-level wind comfort analysis (Barlow et al. ,Cantwell, B. Forte, M., et al).A pressure tap system that introduces measurement errors — through channel occlusion, pneumatic leak, or excessive pressure transmission lag attributable to excessive conduit length or restriction — compromises the quality of the experimental data regardless of the accuracy with which the flow is simulated (Snyder, J.C., et al. (2015), Tamura et al., 1998). The fabrication of pressure-instrumented models for BLWT experiments has historically relied on CNC subtractive machining of wood, engineering polymers, or aluminum, with pressure channels drilled individually into the prefabricated body along straight trajectories accessible to the drill bit. The drill-access constraint limits channel routing to straight-line trajectories, restricting tap density on curved surfaces and precluding the branching manifold geometries that would minimize conduit length and associated pneumatic lag (Ortyl, J., Topa, M., et al. (2019), Ortyl, J., Wilamowski, J., et al. (2015), Ortyl, J. and Popielarz, R. (2012). These limitations are particularly acute in motorsport and complex architectural applications, where geometric complexity is high and rapid iteration is essential. Additive manufacturing (AM) technologies have emerged over the past decade as a fabrication paradigm with the potential to address these constraints systematically. (Al Mousawi, A., Dietlin, C., et al. (2016), Ortyl, J., Sawicz, K., et al. (2015). In DLP fabrication, a UV projector sequentially cures thin layers of liquid photopolymer resin, building the part layer by layer directly from a three-dimensional digital geometry (Tomal, W., et al. 2021, Topa, M., Ortyl, J., et al. (2018,2023). Internal voids, channels, and manifolds of any routing complexity are produced simultaneously with the surrounding solid structure, without any additional tooling or post-fabrication operations, provided that the fabrication parameters are appropriately controlled.

2. METHODOLOGY

To investigate the flow characteristics of pressure channels fabricated by DLP 3D printing using a newly developed photocurable material (currently under patent preparation), and to assess their impact on the accuracy of pressure measurements in wind tunnel testing, a series of model pressure channel segments was prepared. The channels had a diameter of approximately 0.8 mm, a length of approximately 5 cm, and various geometries, including a straight section and bends of 15°, 30°, 45°, 60°, 90°, 120°, 150°, 180°, as well as segments with multiple bends (with a total length of 10 cm). At the outlet of each channel segment, dedicated connectors were designed to enable connection to standard silicone pressure tubes (inner diameter 0.8 mm, outer diameter 1.1 mm). A standard DLP 3D printer (ELEGOO Mars 4 DLP) was used for fabrication. The standard layer exposure time was 2 s, the bottom layer exposure time was 30 s, the number of bottom layers was 5, and the layer thickness was 0.03 mm. The light intensity was 4 mW/cm² at a wavelength of 405 nm. After printing, the channels were subjected to ultrasonic cleaning for approximately 5 minutes and subsequently flushed with isopropanol under a pressure of approximately 1.5–2 bar. The prepared pressure channels were then connected, using silicone tubing, to a multi-channel pressure scanner and mounted on a measurement plate in the wind tunnel (mixed-circuit wind tunnel of the Wind Engineering Laboratory at the Cracow University of Technology), with the channel outlets oriented in the direction of airflow. Additionally, a reference point pressure sensor connected only via a standard silicone tube was installed on the measurement plate. Prior to the main aerodynamic measurements, the wind velocity profile and turbulence intensity profile of the wind tunnel were determined. Measurements were carried out at wind speeds of 4, 6, 8, 11, 13, and 15 m/s, under terrain category I conditions (without turbulence-generating elements such as blocks or spires), recording pressure values from the multi-channel scanner relative to the reference pressure, in accordance with standard aerodynamic testing procedures.

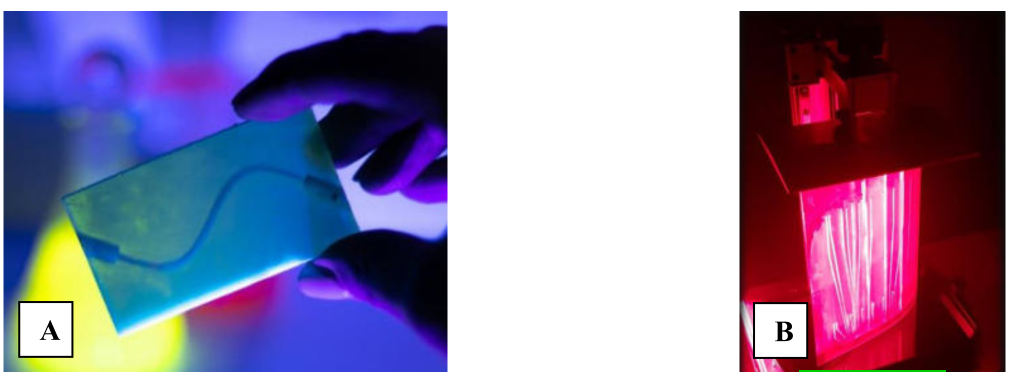

Figure 1. DLP-printed model featuring an internally designed pressure channel - 2 waves sinusoidal channel (A) and DLP-printed photopolymer aerodynamic test model with an integrated internal pressure channel, visible through the translucent resin body in red light, demonstrating the capability of the process to reproduce complex curved conduit trajectories as a monolithic component without post-fabrication drilling (B).

3. RESULTS AND DISCUSSION

The results presented in Fig. 2 demonstrate a pronounced dependence of the measured pressure values on the geometry of the pressure channels fabricated using DLP technology. This effect is consistent across the entire investigated wind velocity range (4–15 m/s), indicating that the observed trends are governed primarily by geometric flow resistance rather than flow regime transitions.

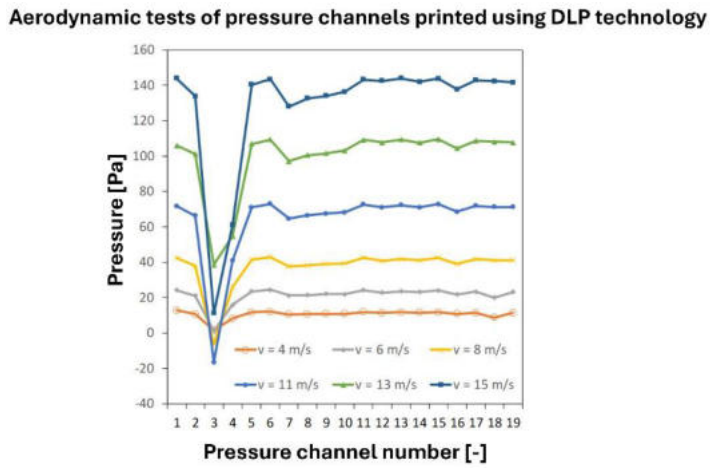

Figure 2. Pressure values recorded by the multi-channel pressure scanner at different wind speeds in the wind tunnel for all analyzed geometries of 3D-printed pressure channels fabricated from the developed photocurable material, where: 1 – reference, 2 – 180° single bend, 3 – 180° double bend, 4 – 150° single bend, 5 – 120° single bend, 6 – 90° single bend, 7 – 60° single bend, 8 – 45° single bend, 9 – 30° single bend, 10 – 15° single bend, 11 – straight section, 12 – sinusoidal channel (1 wave), 13 – sinusoidal channel (2 waves), 14 – sinusoidal channel (3 waves), 15 – sinusoidal channel (4 waves), 16 – sinusoidal channel (8 waves), 17 – two 90° bends separated by a 2 cm straight section, 18 – two 90° bends separated by a 5 cm straight section, 19 – two 90° bends separated by a 10 cm straight section.

The reference configuration (Channel 1, straight path without disturbances) consistently yields the highest-pressure values for all velocities, confirming that it represents the baseline with minimal hydraulic losses. Any deviation from this geometry introduces additional flow resistance, manifested as a reduction in recorded pressure. A distinct and systematic pressure drop is observed for geometries incorporating sharp directional changes, particularly for channels with 180° bends (Channels 2 and 3). Among all tested configurations, these geometries produce the lowest pressure values, with the double 180° bend (Channel 3) exhibiting the most significant pressure attenuation. This behavior is attributed to strong local flow separation, recirculation zones, and increased energy dissipation associated with abrupt flow reversal. For single-bend geometries (Channels 4–10), a clear relationship between bending angle and pressure loss is evident. As the bend angle decreases from 150° to 15°, the measured pressure gradually approaches the reference values. This indicates that smoother flow redirection results in lower energy losses. However, even relatively mild bends (e.g., 30° or 15°) still introduce measurable pressure deviations compared to the straight channel, highlighting the sensitivity of the system to even minor geometric perturbations. The straight section (Channel 11) yields result very close to the reference, confirming that pressure losses due to friction alone (in the absence of curvature) are negligible compared to losses induced by geometric disturbances. More complex geometries, such as sinusoidal channels (Channels 12–16), show intermediate behavior between straight and sharply bent configurations. The pressure loss increases with the number of sinusoidal waves, indicating cumulative effects of repeated curvature. Channels with higher wave counts (e.g., 4 and 8 waves) exhibit noticeable pressure attenuation, although still significantly less severe than in the case of 180° bends. This suggests that distributed curvature (as in sinusoidal channels) induces less severe local flow disturbances compared to discrete sharp bends, even when the total flow path length is increased. The energy losses in such geometries are therefore dominated by repeated mild redirections rather than singular, high-intensity flow disruptions. Channels containing multiple bends separated by straight sections (Channels 17–19) reveal an additional geometric effect related to spacing between disturbances. Increasing the distance between two 90° bends leads to a gradual recovery of pressure values.

4. CONCLUSIONS

The obtained results clearly demonstrate that the geometry of internal pressure channels in DLP-fabricated aerodynamic models can significantly influence measured pressure values. Inaccurate channel design may therefore introduce systematic measurement errors, especially in configurations involving sharp bends (180°) or complex trajectories (multiple closely spaced bends). From a practical standpoint, the following design guidelines can be formulated: 1 - Straight or near-straight channels should be preferred whenever possible to minimize pressure losses; 2 - Sharp bends (especially 180°) should be avoided due to severe flow disturbances; 3 - If curvature is necessary, gradual bends or distributed geometries (e.g., sinusoidal paths) are preferable; 4 - Adequate spacing between successive bends should be ensured to allow flow recovery. Within the scope of this study, it has been demonstrated that, by following the proposed design guidelines for internal pressure channels, it is possible to successfully fabricate such channels together with the tested models in a single DLP 3D printing process using photocurable resins with appropriately optimized compositions (i.e. a sufficiently high density-to-viscosity ratio), without adversely affecting the pressure values obtained during aerodynamic testing. These findings are critical for the design of integrated pressure channel networks in additively manufactured aerodynamic models, particularly when high measurement accuracy is required.

5. ACKNOWLEDGEMENTS

The research was conducted as part of the Proof of Concept project (contract no. FENG.02.07-IP.05-0451/23), funded by the Foundation for Polish Science, entitled "New polymer-based Pressure Sensitive Paint (PSP) sensory systems for aerodynamic testing aimed at accurate prediction of the impact of building structures on the risk of adverse atmospheric phenomena and pedestrian wind comfort in urban areas" and LIDER XII project (agreement no. LIDER/51/0270/L-12/20/NCBR/2021) titled „Multi-material 3D printer dedicated to production of solid metal and galvanic alloys parts, as well as metal-polymer hybrid elements using developed coupled technology of metal electrodeposition and photopolymerization of polymer resins" funded by the National Centre for Research and Development.

6. REFERENCES

Al Mousawi, A., Dietlin, C., et al. (2016). Meta-Terphenyl Derivative/Iodonium Salt/9H-Carbazole-9-ethanol Photoinitiating Systems for Free Radical Promoted Cationic Polymerization upon Visible Lights. Macromolecular Chemistry and Physics 217(17), pp. 1955–1965.

Barlow, J.B., et al. (1999). Low-Speed Wind Tunnel Testing. 3rd ed. Wiley-Interscience.

Cantwell, B. and Coles, D. (1983). An experimental study of entrainment and transport in the turbulent near wake of a circular cylinder. Journal of Fluid Mechanics 136, pp. 321–374.

Forte, M., et al. (2015). Numerical and experimental analysis of roughness-induced transition. Procedia IUTAM

Ortyl, J. and Popielarz, R. (2012). New photoinitiators for cationic polymerization. Polymers 57(7-8),

Ortyl, J. and Popielarz, R. (2013). The performance of 7-hydroxycoumarin-3-carbonitrile and 7-hydroxycoumarin-3-carboxylic acid as fluorescent probes for monitoring of cationic photopolymerization processes by FPT. Journal of Applied Polymer Science 128(3), pp. 1974–1978.

Ortyl, J., Sawicz, K., et al. (2010). Performance of amidocoumarins as probes for monitoring of cationic photopolymerization of monomers by fluorescence probe technology. Journal of Polymer Science Part A: Polymer Chemistry 48(20), pp. 4522–4528.

Ortyl, J., Wilamowski, J., et al. (2015). Relative sensitization efficiency of fluorescent probes/sensitizers for monitoring and acceleration of cationic photopolymerization of monomers. Polymer Testing 48

Ortyl, J., Topa, M., et al. (2019). Mechanism of interaction of aminocoumarins with reaction medium during cationic photopolymerization of triethylene glycol divinyl ether. European Polymer Journal 116, pp. 45–55.

Snyder, J.C., et al. (2015). Build direction effects on additively manufactured channels. Journal of Turbomachinery 138(5).

Stathopoulos, T. (1984). Design and fabrication of a wind tunnel for building aerodynamics. Journal of Wind Engineering and Industrial Aerodynamics 16(2-3), pp. 361–376.

Tamura, T., et al. (1998). Numerical prediction of unsteady pressures on a square cylinder with various corner shapes. Journal of Wind Engineering and Industrial Aerodynamics 74-76, pp. 531–542.

Tieleman, H.W. (2003). Wind tunnel simulation of wind loading on low-rise structures: A review. Journal of Wind Engineering and Industrial Aerodynamics 91(12-15), pp. 1627–1649.

Tomal, W., Krok, D., et al. (2021). Harnessing light to create functional, three-dimensional polymeric materials: multitasking initiation systems as the critical key to success. Additive Manufacturing 48, 102447.

Topa, M., Ortyl, J., et al. (2018). Applicability of samarium(III) complexes for the role of luminescent molecular sensors for monitoring progress of photopolymerization processes and control of the thickness of polymer coatings. Spectrochimica Acta Part A: Molecular and Biomolecular Spectroscopy 199, pp. 430–440.

Topa-Skwarczyńska, M. and Ortyl, J. (2023). Photopolymerization shrinkage: strategies for reduction, measurement methods and future insights. Polymer Chemistry 14(18), pp. 2145–2158.